

Wormhole Model for Neon-20

Nicholas S. Manton¹ and Maciej Dunajski²

*Department of Applied Mathematics and Theoretical Physics,
University of Cambridge,
Wilberforce Road, Cambridge CB3 0WA, U.K.*

Abstract

A quantum mechanical model for the Neon-20 nucleus is developed that allows for the splitting of a bipyramidal structure of five alpha-partices into an alpha-particle and an Oxygen-16 nucleus. The geometry of the configuration space is assumed to be a 3-dimensional spatial wormhole, and on the wormhole background there is an attractive short-range potential. This leads to a radial Schrödinger equation of the Heun form, which simplifies for threshold bound states to an associated Legendre equation that has explicit solutions. The energies of the true bound states for all spin/parities are numerically calculated, and match those of the well-established $K^\pi = 0^+$, $K^\pi = 0^-$, and certain higher rotational bands of Neon-20.

Keywords: Spatial Wormhole, Neon-20 Nucleus, Rotational Bands

¹email: N.S.Manton@damtp.cam.ac.uk

²email: M.Dunajski@damtp.cam.ac.uk

1 Motivation

We develop a model for quantum states of the Neon-20 nucleus, where the underlying configuration space is a spatial wormhole. Spacetime wormholes have generated much interest, but are usually regarded as a science-fiction fantasy. Here we find a wormhole that is physically realised – not as a space-time, but as a model configuration space for a spatially-extended, deformable nucleus. The characteristic length scale of the wormhole is about 5 fm, comparable to the size of the Neon-20 nucleus. This wormhole model was first outlined in [1], but not analysed there in any detail.

We start from the old idea that the ground-state configuration of Neon-20 is a bipyramid of five alpha-particles [2, 3, 4], which splits relatively easily into a single alpha-particle and a bound cluster of four alpha-particles representing Oxygen-16. The bipyramid has an equilateral triangle of alphas in the middle, but we ignore rotations in the plane of this triangle and treat the bipyramid as axially symmetric. The angular momentum projection about the symmetry axis is therefore $K = 0$. We also neglect centre of mass motion.

Conventionally, one would have a Euclidean configuration space for the separation vector of the two clusters. A central ball can then be cut out to enforce a non-zero minimal separation, or a potential can be introduced that strongly disfavours the clusters from overlapping. Such models have rather singular behaviour near the bipyramid.

In contrast, our model has a smooth, curved configuration space near the bipyramid, avoiding any singularity. It has a single radial coordinate r , which accurately corresponds to the separation of the clusters asymptotically, when they are well-separated, and additionally has the usual spherical polar coordinates (θ, ϕ) representing the direction of the separation axis. Unusually, however, r runs from $-\infty$ to ∞ . The metric is that of an Ellis–Bronnikov wormhole [5, 6]

$$ds^2 = dr^2 + (r^2 + a^2)(d\theta^2 + \sin^2 \theta d\phi^2). \quad (1)$$

On this background, there is a smooth, attractive potential energy depending symmetrically on r , with its minimum at $r = 0$ where the clusters merge into the bipyramid. The radius of the wormhole’s throat, a , is related to the linear size of the bipyramid.

To justify this geometry, consider a simple classical motion with r monotonically decreasing through zero, and (θ, ϕ) fixed. This models an incoming alpha-particle coalescing instantaneously with the four-alpha cluster to form the bipyramid, and a different alpha-particle from the opposite side of the bipyramid getting ejected. The motion can be thought of as analogous to

that of a Newton cradle, with one ball coming in and a different ball going out. If the incoming and outgoing alpha-particles are distinguishable, it makes sense for r to have the range $(-\infty, \infty)$. However, note that the outgoing particle's angular coordinates are antipodal to those of the incoming particle, and because alpha-particles are indistinguishable bosons, one should identify points in configuration space with coordinates (r, θ, ϕ) and $(-r, \pi - \theta, \phi + \pi)$. The true configuration space is therefore not the complete wormhole, but its quotient by \mathbb{Z}_2 under this identification.

The \mathbb{Z}_2 action has no fixed points, so the quotient space is smooth. The quotient is the half-wormhole $r \geq 0$, where antipodal points (θ, ϕ) and $(\pi - \theta, \phi + \pi)$ on the 2-sphere at $r = 0$ are identified. This identification is required, because the bipyramid is symmetric under the antipodal map. We will quantize the dynamics on the half-wormhole, but to do this it is convenient to perform the quantization on the complete wormhole, separating radial and angular variables as usual; the \mathbb{Z}_2 symmetry then constrains physical states to be either symmetric in r with even angular momentum, or antisymmetric in r with odd angular momentum. A state's parity is even/odd if the angular momentum is even/odd.

This wormhole model is an anharmonic extension of a rovibrational model for Neon-20, incorporating only the lowest-frequency vibrational mode of the bipyramid, the singly-degenerate mode transforming under the A_2'' representation of \mathcal{D}_{3h} that tends to produce a 1+4 cluster split. The mode's oscillating amplitude corresponds to an oscillation of r around zero. The potential on the wormhole is minimal at the bipyramid, just like the harmonic oscillator potential. Another similarity is that the quantized rovibrational model has a bosonic constraint. Physical states are those with either an even number of vibrational phonons and even angular momenta, or an odd number of phonons and odd angular momenta.

Apart from the wormhole radius a , our model has just one adjustable, dimensionless parameter m . It can take any positive value, and we found initially that a good fit to experimental data was with $m = 9.01$. Mathematically, it is very convenient for m to be a positive integer, so we have fixed $m = 9$. A consequence is that all the threshold bound states, just below the continuum scattering states, have radial wavefunctions given by analytic solutions of an associated Legendre equation.

Having fixed $m = 9$, together with an energy scale, we obtain a good match to the lowest observed rotational bands of Neon-20 with quantum numbers $K^\pi = 0^+$ and $K^\pi = 0^-$, interpreted here as zero-phonon and one-phonon bands. Bijker and Iachello have presented a rovibrational analysis of Neon-20 states, incorporating all modes of small oscillation of the bipyramid [7]. Our interpretation of some of the higher $K = 0$ bands differs somewhat

from theirs. We agree on the two-phonon 0^+ band, but interpret the second 0^- band as a three-phonon band, rather than a band combining two distinct phonons with opposite \mathbb{Z}_2 symmetries. Quantitatively, our results are comparable, but as we have fewer adjustable parameters, we can predict some of the parameters that they have fitted – in particular, the ratios of the rotational constants B associated to the various $K = 0$ bands.

2 Quantum States on the Wormhole

We start with the classical Lagrangian dynamics for the relative motion of an alpha-particle and a four-alpha cluster, and then quantize. The Lagrangian is

$$L = \frac{1}{2}\mu \left(\dot{r}^2 + (r^2 + a^2)(\dot{\theta}^2 + \sin^2 \theta \dot{\phi}^2) \right) + \frac{V_0}{(r^2 + a^2)^2}, \quad (2)$$

where the kinetic term is based on the wormhole metric, μ is the reduced mass of the two clusters at large separation, and V_0 is a positive constant so the potential is negative and attractive. The physical interpretation of the wormhole geometry is that the inertial mass tensor is separation-dependent, and different in the radial and angular directions. A separation-dependent inertial mass in the radial direction has been previously considered in the context of Neon-20 by Wen and Nakatsukasa [8].

The quantum Hamiltonian derived from L is

$$\begin{aligned} H &= -\frac{\hbar^2}{2\mu} \nabla^2 - \frac{V_0}{(r^2 + a^2)^2} \\ &= -\frac{\hbar^2}{2\mu} \left(\partial_{rr} + \frac{2r}{r^2 + a^2} \partial_r + \frac{1}{r^2 + a^2} \nabla_{\text{ang}}^2 \right) - \frac{V_0}{(r^2 + a^2)^2}, \end{aligned} \quad (3)$$

where ∇^2 is the Laplace–Beltrami operator for the wormhole metric (1), and ∇_{ang}^2 is the usual angular part of the Laplacian in spherical polars. ∇^2 reduces to the standard Laplacian in spherical polars when $a = 0$. We separate variables, and write stationary state wavefunctions as

$$\Phi(r, \theta, \phi) = \chi(r) Y_{l, \tilde{m}}(\theta, \phi). \quad (4)$$

l is the usual angular momentum quantum number, and the index \tilde{m} takes its usual $2l+1$ values. We are reserving m to be a parameter in the potential. The reduced, radial equation for stationary states of energy E is

$$-\frac{\hbar^2}{2\mu} \left(\frac{d^2 \chi}{dr^2} + \frac{2r}{r^2 + a^2} \frac{d\chi}{dr} - \frac{l(l+1)}{r^2 + a^2} \chi \right) - \frac{V_0}{(r^2 + a^2)^2} \chi = E \chi. \quad (5)$$

We recall that bound states of the potential $V = \text{const} \cdot (r^2 + a^2)^{-2}$ with zero angular momentum have, in the context of kinks on the wormhole background, been considered in [9] and [10].

We now change variable by setting $r = ax$, and write $V_0 = \frac{\hbar^2 a^2}{2\mu} m^2$ and $E = \frac{\hbar^2}{2\mu a^2} \varepsilon$. The radial equation then has the dimensionless form

$$-\frac{d^2\chi}{dx^2} - \frac{2x}{x^2+1} \frac{d\chi}{dx} + \frac{l(l+1)}{x^2+1} \chi - \frac{m^2}{(x^2+1)^2} \chi = \varepsilon \chi. \quad (6)$$

Equation (6) for general ε is a confluent Heun equation, with two regular singular points at $x = \pm i$, and a confluent singularity at infinity. Its general solution is given by

$$\begin{aligned} \chi(x) = & c_1 (x^2 + 1)^{\frac{m}{2}} \text{HeunC} \left(0, -\frac{1}{2}, m, -\frac{\varepsilon}{4}, \frac{m^2+1-l(l+1)+\varepsilon}{4}, -x^2 \right) \\ & + c_2 x (x^2 + 1)^{\frac{m}{2}} \text{HeunC} \left(0, \frac{1}{2}, m, -\frac{\varepsilon}{4}, \frac{m^2+1-l(l+1)+\varepsilon}{4}, -x^2 \right). \end{aligned} \quad (7)$$

There is more than one motivation for our choice of potential. It is short-ranged compared to the centrifugal repulsion proportional to $l(l+1)$ (although not exponentially so). It is a multiple of the Ricci scalar curvature of the wormhole, something that could arise from an alternative treatment of canonical quantization. Finally, the potential's algebraic form means that for $\varepsilon = 0$, eq.(6) usefully simplifies to the associated Legendre equation, which can be explicitly solved.

3 The Energy Spectrum

Here we derive some general properties of the bound state spectrum of the radial equation (6). True bound states are solutions with negative ε , but there are also normalisable, threshold bound states with $\varepsilon = 0$.

If we write $\chi(x) = (x^2 + 1)^{-\frac{1}{2}} \eta(x)$, eq.(6) becomes

$$-\frac{d^2\eta}{dx^2} + \frac{l(l+1)}{x^2+1} \eta - \frac{m^2-1}{(x^2+1)^2} \eta = \varepsilon \eta, \quad (8)$$

which is easier to treat analytically. The transformed equation (8) is a 1-d Schrödinger equation with effective potential (Fig.1)

$$v_{\text{eff}}(x) = \frac{l(l+1)}{x^2+1} - \frac{m^2-1}{(x^2+1)^2}. \quad (9)$$

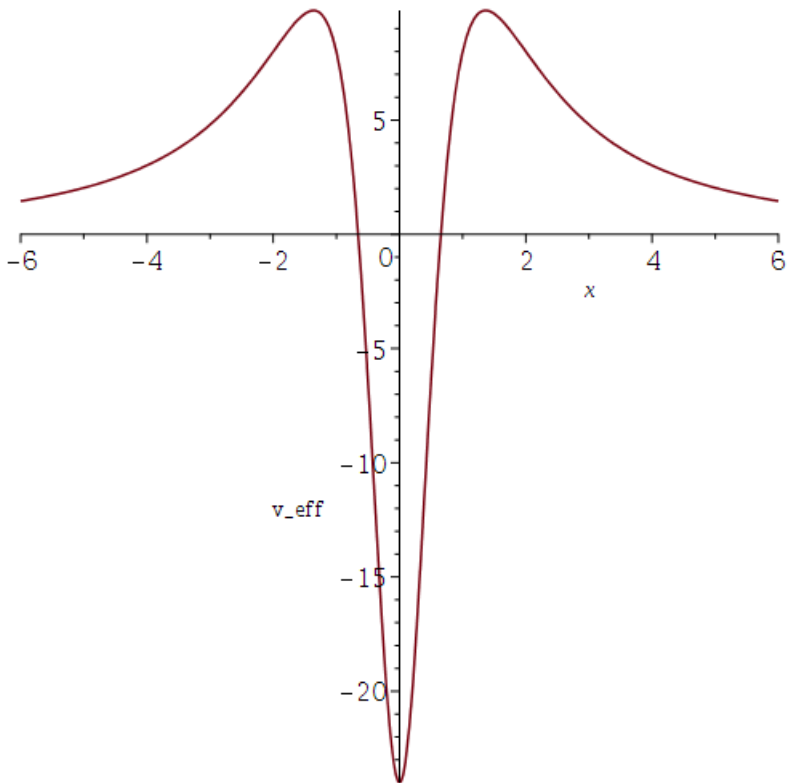


Figure 1. Effective potential with $m = 9$ and $l = 7$.

For bound states to exist, v_{eff} has to be negative somewhere, which requires $m^2 - 1 > l(l+1)$. On the other hand, if $m^2 - 1 > 2l(l+1)$ then the integral of v_{eff} over \mathbb{R} is negative, and a bound state definitely exists (by a variational argument). For general positive m we therefore expect bound states, but only for $l < m$.

Rather remarkably, there are threshold bound states for all $0 < l < m$ when m is a positive integer. To see this, we rewrite eq.(6) for $\varepsilon = 0$ as

$$(x^2 + 1) \frac{d^2 \chi}{dx^2} + 2x \frac{d\chi}{dx} - l(l+1) \chi + \frac{m^2}{x^2 + 1} \chi = 0. \quad (10)$$

Setting $z = ix$, this becomes the standard associated Legendre equation. We are interested in solutions for real x that are normalisable, and these are associated Legendre functions evaluated on the imaginary z -axis. As this axis does not pass through the regular singular points at $z = \pm 1$, the solutions can be singular at these points, and we are not constrained to impose $|m| \leq l$ as in the construction of spherical harmonics.

We can therefore assume that χ has the form

$$\chi(x) = \frac{S(x)}{(x^2 + 1)^{\frac{m}{2}}} \quad (11)$$

where

$$S(x) = \sum_{k=0} a_k x^k. \quad (12)$$

From (10) we then derive the recurrence relation

$$a_{k+2} = -\frac{m(m-1) - l(l+1) - (2m-1)k + k^2}{(k+2)(k+1)} a_k. \quad (13)$$

$\chi(x)$ is the radial wavefunction of a normalisable, threshold bound state provided the series for S truncates to a finite polynomial of degree less than $m-1$. This occurs for all angular momenta in the range $0 < l < m$, and we denote the resulting polynomial $S_l^m(x)$. S_l^m has degree $m-l-1$. It is even if $m-l-1$ is even and odd if $m-l-1$ is odd, and has $m-l-1$ nodes. A further threshold state exists for $l=0$, but this is not normalisable because S has degree $m-1$. Note that all the threshold states are physically allowed provided m is odd, because $m-l-1$ has the same parity as l in this case.

As explained in Sect.1, we have made the choice $m=9$. Usefully, for fitting the Neon-20 spectrum, there are then threshold states for all angular momenta up to $l=8$. For $m=9$, and l decreasing from 8 to 1 the polynomials $S_l^9(x)$ are respectively

$$\begin{aligned} &1, \ x, \ 1-15x^2, \ 3x-13x^3, \ 3-78x^2+143x^4, \ 15x-110x^3+99x^5, \\ &5-165x^2+495x^4-231x^6, \ 5x-45x^3+63x^5-15x^7, \\ &1-36x^2+126x^4-84x^6+9x^8, \end{aligned} \quad (14)$$

and all their roots are real.

$\chi(x)$ is in fact, up to a normalisation constant, the associated Legendre function of the second kind $Q_l^m(z)$, evaluated on the imaginary axis $z=ix$. It has the explicit form, for m an integer greater than l ,

$$Q_l^m(z) = (1-z^2)^{\frac{m}{2}} \frac{d^m}{dz^m} \left[\ln \left(\frac{1+z}{1-z} \right) \frac{d^l}{dz^l} (1-z^2)^l \right]. \quad (15)$$

One might anticipate, from the expression for $Q_l(z)$ in ref.[11], an additional polynomial inside the square brackets, but its m th derivative vanishes. Also, because $m > l$, at least one derivative acts on the logarithmic term, so there is no such term in the result.

Let us now consider the negative energy bound states. Because the threshold bound state with angular momentum l has $m - l - 1$ nodes, it follows from the Sturm oscillation theorem that there are $m - l - 1$ negative energy states with angular momentum l . These are confluent Heun functions, but as there are no simple formulae for their energies, we have solved eq.(8) numerically to find them. We use a shooting and bisection method on the interval $[-20, 20]$, using as initial condition at $x = 0$ either that η has zero slope (for the even solutions) or zero value and a finite slope (for the odd solutions).

For each l , the lowest-energy wavefunction $\eta(x)$ is symmetric in x and has no nodes, but as the energy increases, the parity of η alternates and the number of nodes increases by 1. The physically allowed states are those where the parity of η matches the parity of l . The spectrum of physically allowed states for $m = 9$, including all the threshold states, is shown in Fig.2.

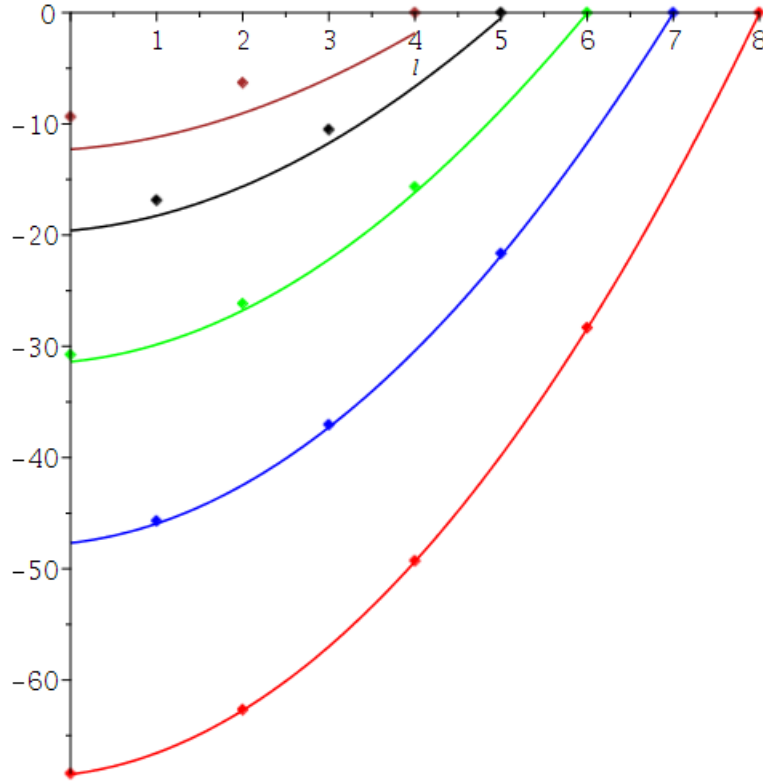


Figure 2. Numerical bound state spectrum for $m = 9$ and integer $l < 9$ (dots), compared with the anharmonic oscillator approximation (curves).

Although the true energies of the bound states are not known analytically, they can be evaluated using an anharmonic oscillator approximation. The

expansion of v_{eff} up to $O(x^4)$ is

$$v_{\text{eff}} \simeq -(m^2-1)+l(l+1)+[2(m^2-1)-l(l+1)]x^2-[3(m^2-1)-l(l+1)]x^4. \quad (16)$$

Using the harmonic oscillator wavefunctions for v_{eff} truncated at order x^2 , together with first-order perturbation theory to take account of the x^4 term [12], we find the approximate energy levels

$$\begin{aligned} \varepsilon_{n,l} = & -(m^2-1)+l(l+1)+(2n+1)\sqrt{2(m^2-1)-l(l+1)} \\ & -\frac{3}{2}\frac{3(m^2-1)-l(l+1)}{2(m^2-1)-l(l+1)}\left(n^2+n+\frac{1}{2}\right), \end{aligned} \quad (17)$$

where $n \geq 0$ is the harmonic oscillator level. These approximate energies are also shown in Fig.2 for $m = 9$, as functions of continuous l . The lowest-lying states for each even l comprise the ground state rotational band, with $n = 0$, and above this we see the higher rotational bands. The n th rotational band can be interpreted as rotational excitations of an n -phonon, purely vibrational state.

For $m = 9$, the anharmonic oscillator energies are accurate only up to about $n = 4$, but the phonon number n is still a good label for all the bound states. The rotational bands get shorter as n increases, because the threshold state is reached when $l = 8 - n$.

In each rotational band, we can express the energy for small l as

$$\varepsilon_{n,l} \simeq \varepsilon_n + b_n l(l+1), \quad (18)$$

where b_n is the rotational constant (inversely proportional to the effective moment of inertia of the band). The anharmonic oscillator approximation gives, for $m = 9$,

$$b_n \simeq 1 - \frac{1}{\sqrt{640}}(2n+1) - \frac{3}{640}\left(n^2+n+\frac{1}{2}\right). \quad (19)$$

The values for the lowest few bands are $b_0 = 0.96$, $b_1 = 0.86$, $b_2 = 0.77$, $b_3 = 0.66$ and $b_4 = 0.54$. We see from Fig.2 that these are quite accurate, even though the actual rotational bands are significantly shifted up for $n = 3$ and $n = 4$.

A selection of bound state wavefunctions $\eta(x)$ is shown in Figs.3a, 3b, 3c.

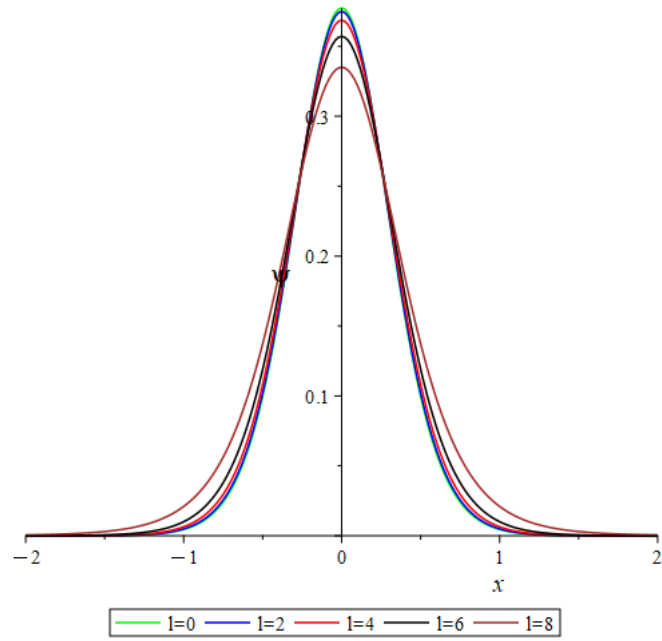


Figure 3a. Bound states with $n = 0$.

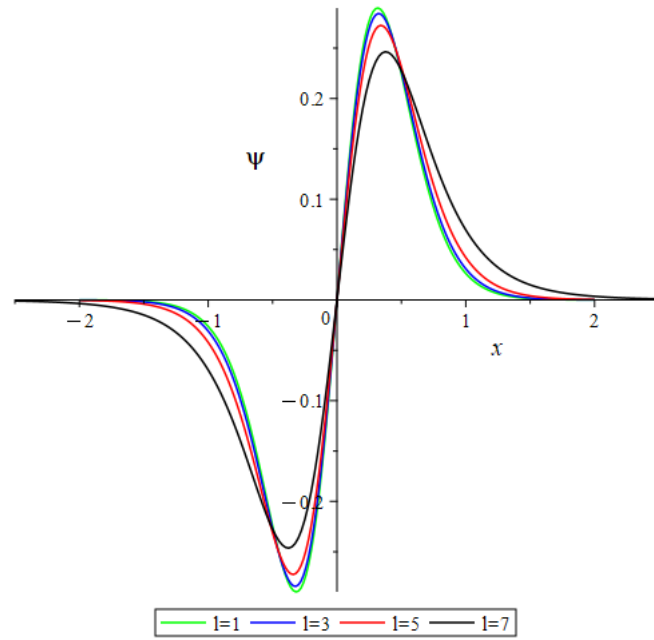


Figure 3b. Bound states with $n = 1$.

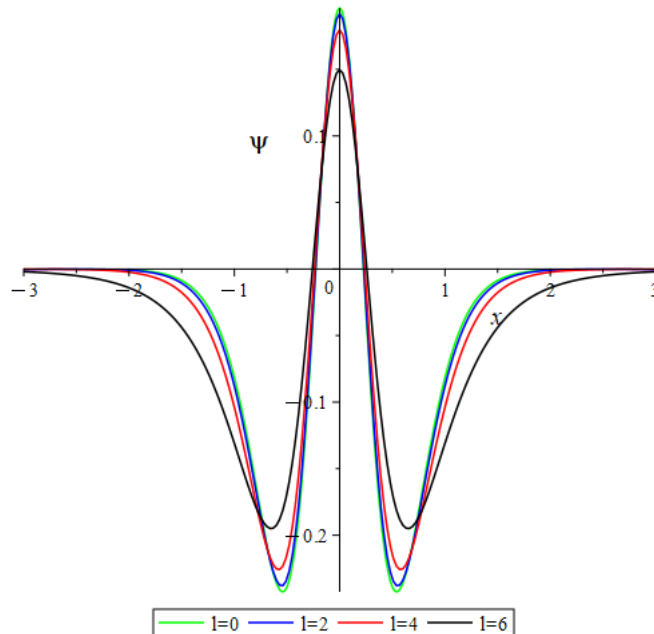


Figure 3c. Bound states with $n = 2$.

For given n , and independently of l , they have n nodes in the full range $-\infty < x < \infty$ and their widths hardly change with l because they are well approximated by harmonic oscillator wavefunctions in the simplified, l -independent effective potential derived from (9),

$$\widetilde{v}_{\text{eff}} = -m^2 + 2m^2x^2. \quad (20)$$

However, the threshold states, with maximal l , are broader and decay more slowly for large $|x|$.

These wavefunctions may be compared to those in refs.[13] and [14], whose node number varies with l . However, most of the latter nodes are in the cluster-overlap region, and the wormhole wavefunctions are similar in shape if the comparison is made outside this region.

4 Comparison with Neon-20 States

For the experimental spectrum of Neon-20, we use the TUNL tables [15]; see also the review [16] and the ENSDF tables [17]. The identification of rotational bands in Neon-20 goes back many decades. See, for example,

refs.[18, 19, 14, 20, 21] among many others, also Table 20.20 in [16], and the recent discussion by Bijker and Iachello [7]. The ground state 0_1^+ rotational band is well established up to $l = 6$. There is also a well-established, lowest 0^- rotational band with states from $l = 1$ up to $l = 7$. We identify these bands with the 0-phonon and 1-phonon bands in our model. There are a few more recognised 0^+ bands. Following Bijker and Iachello, we regard the 0_2^+ and 0_3^+ bands as arising from other, symmetric vibrational excitations of the bipyramid, and identify the experimental 0_4^+ band as the 2-phonon band in our model. The states of the 0_4^+ band have been recognised as “higher nodal” states by Fujiwara et al. [14], and our model gives them the expected wavefunction structure, with a single node in the half-wormhole range $x > 0$. We have also tentatively identified one higher, observed rotational band with the 3-phonon band of our model. A few further observed states can be assigned to the shorter bands with 4-, 5-, 6- and 7-phonons. 0^+ bands have positive-parity states of even angular momenta, and 0^- bands have negative-parity states of odd angular momenta.

To calibrate our model, we need to shift the model ground state upwards to match the experimental energy $E = 0$, and then find the optimal physical energy scale $\hbar^2/2\mu a^2$ by a least squares fit. The model’s dimensionless ground state energy is $\varepsilon = -68.5$ (both numerically and in the anharmonic oscillator approximation) so the shift upwards is by 68.5.

In a preliminary fit we matched the states that are most confidently assigned to rotational bands – those in the ground state 0_1^+ band up to 6^+ , the lowest 0^- band up to 7^- , and the 0_4^+ band up to 4^+ . Following refs.[14, 21] and others, we identified the 7^- state at 15.37 MeV to be in the 0^- band; it is a threshold state in our model. Consistently with this, the preliminary fit gave a threshold energy just above 15 MeV. We then noted that the states in the TUNL table between 15.1 MeV and 15.9 MeV are unique candidates for all the threshold states in our model, with spin/parities between 1^- and 8^+ . All the required spin/parities occur, and there are almost no other observed states in this energy range, one exception being the 8^- state assigned to the 2^- band of Neon-20.

For our final calibration, we therefore extended our ground state rotational band to include the 15.87 MeV 8^+ state as the threshold state. Other models also predict that the 8^+ state in the ground state band has a similar energy [13]. There is one lower 8^+ state at 11.95 MeV that is often assigned to the ground state band, but this creates a sharp kink in the band slope, and the state has other properties that makes this assignment controversial, for example, its rather low E2 transition rate to the 6^+ state in the ground state band [16]. We also followed Michel et al. [22] in assigning the 15.16 MeV 6^+ state to the observed 0_4^+ band of broad, higher nodal states. They

argued that the energy of the 6^+ state in this band is in the range 14-15 MeV, rather than at 12.58 MeV. It becomes the threshold state in our 2-phonon band. The broad 5^- state at 15.17 MeV becomes the threshold state in the 3-phonon band. We have also identified various lower-spin states in the TUNL table that are close in energy to the states required for our model, both at and below the threshold, but these states are more numerous, so we have some choice, and they have less significance.

In the best fit of our model to all these 24 identified states, the conversion factor from the shifted ε to the physical energy E is $\hbar^2/2\mu a^2 = 0.222$ MeV. The threshold energy is then at $E_{\text{thresh}} = 68.5 \times 0.222 \text{ MeV} = 15.19$ MeV. Setting $\hbar = 197.3$ MeV fm, and $\mu = 2982$ MeV (the reduced mass μ being almost exactly four-fifths of the alpha-particle mass m_α), we find $a = 5.42$ fm. This is the radius of the 2-sphere throat of the wormhole, and has order of magnitude the linear size of the bipyramid. In Fig.4 we show the best fit of these observed states to our model.

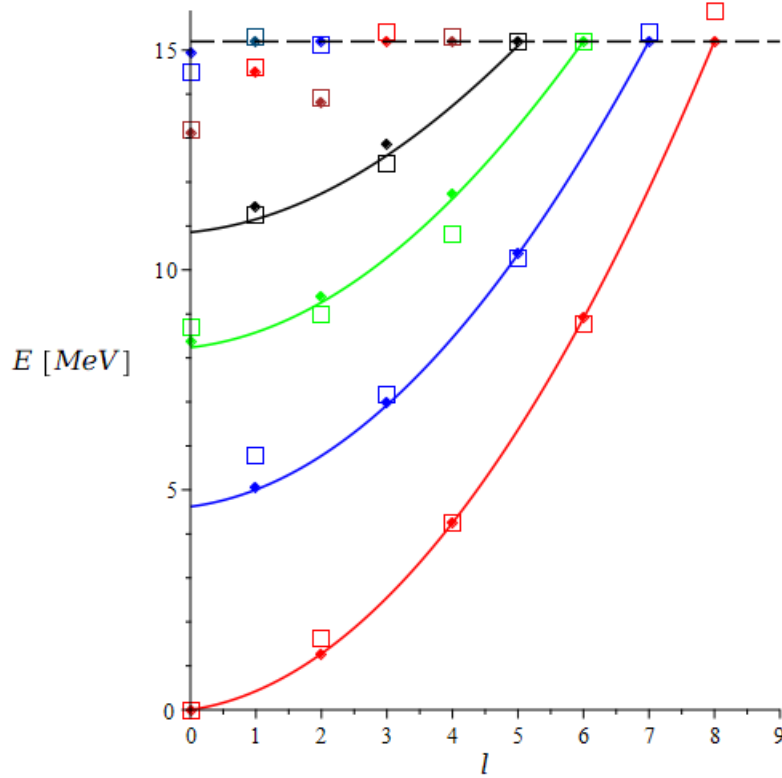


Figure 4. Experimental energies (boxes), numerical bound states (dots), and the anharmonic oscillator approximation (curves).

The dimensionless rotational constant b_n , given in (19), converts to the physical value $B_n = 0.222 b_n$ MeV for the n -phonon band. The rotational

constants of the rotational bands in our model are therefore $B_0 = 0.213(0.212)$, $B_1 = 0.190(0.137)$, $B_2 = 0.170(0.105)$, $B_3 = 0.146(0.101)$ and $B_4 = 0.120$, all in MeV. The bracketed quantities are the rotational constants calculated in ref.[7] for the corresponding bands. Although there are quantitative differences, there is a similar decrease of B_n as n increases.

The detailed comparison between the experimental and model energies in MeV, after the calibration, is as follows:

	Experiment	Model
0-phonon band	[0, 1.63, 4.25, 8.78, 15.87]	[0, 1.28, 4.25, 8.90, 15.19]
1-phonon band	[5.79, 7.16, 10.26, 15.37]	[5.04, 6.97, 10.39, 15.19]
2-phonon band	[8.7, 9.0, 10.8, 15.2]	[8.36, 9.38, 11.71, 15.19]
3-phonon band	[11.25, 12.4, 15.2]	[11.45, 12.86, 15.19]
4-phonon band	[13.2, 13.9, 15.3]	[13.11, 13.80, 15.19]
5-phonon band	[14.6, 15.4]	[14.49, 15.19]
6-phonon band	[14.5, 15.1]	[14.95, 15.19]
7-phonon band	[15.3]	[15.19].

(21)

The TUNL table has no state very close to the model prediction of 14.95 MeV for the 6-phonon 0^+ state. However, a recent review of data from proton/Fluorine-19 scattering experiments [23] identifies some more 0^+ states, including one at 14.9 MeV. This would better fit the 6-phonon band of our model. There are also further 2^+ states identified above 15 MeV, so there is a 15.3 MeV alternative to our choice of the 15.1 MeV state as the threshold 6-phonon state. If we had used these two states in our final calibration, the threshold energy would have been slightly higher.

Identifying the 3-phonon ($n = 3$) band of our model with observed states is rather controversial. We find a good fit to the energies and spin/parities of the observed 0^- band that Bijker and Iachello describe using a combination of antisymmetric and symmetric one-phonon oscillations of alpha-particles along the bipyramid axis. In favour of our interpretation, we note that in earlier work on rovibrational models for Oxygen-16 and Calcium-40 [24, 25], it was found that 3-phonon states of a low-frequency vibrational mode were needed to fit the experimental data. In anharmonic models with a potential that flattens out, 3-phonon states are not of very high energy, and cannot be ignored.

To confirm these band identifications, it would help to have predictions for the frequencies of all vibrational modes of the bipyramid. It would also help to clarify the status of the clear rotational band described as a 1^- band in [16], and interpreted this way in [7]. The problem is that the only experimentally

confirmed states in this band have spin/parities $1^-, 3^-, 5^-, 7^-$, so it looks like a 0^- band. We also note that some of the states assigned to the two double-vibration 0^- bands in [7] are indicated in [16] and in the TUNL table [15] to have isospin 1, rather than the expected isospin 0. Greater clarity concerning the odd spin, negative parity states of Neon-20 would be desirable.

It is of interest to relate the wormhole radius to the bipyramid and two-cluster geometry more concretely using a simplified model. Suppose that pointlike alpha-particles of mass m_α are located at

$$\begin{aligned} (1, 0, \tfrac{1}{4}z) , \left(-\tfrac{1}{2}, \tfrac{\sqrt{3}}{2}, \tfrac{1}{4}z\right) , \left(-\tfrac{1}{2}, -\tfrac{\sqrt{3}}{2}, \tfrac{1}{4}z\right) , (0, 0, \sqrt{2} + \tfrac{1}{4}z) , \\ (0, 0, -\sqrt{2} - z) . \end{aligned} \quad (22)$$

These form a tetrahedral four-alpha cluster centred at $(0, 0, \tfrac{1}{4}(\sqrt{2} + z))$, accompanied by a single alpha-particle at $(0, 0, -(\sqrt{2} + z))$. The cluster separation is $s = \tfrac{5}{4}(\sqrt{2} + z)$. When $z = 0$ these five alphas form a bipyramid of double-tetrahedron shape.

Let us now introduce a spatial scale factor c for this structure. The moment of inertia about any axis through the origin, and orthogonal to the x_3 -axis is found to be

$$\mathcal{I} = \left(\tfrac{4}{5}s^2 + 3\right) m_\alpha c^2 . \quad (23)$$

This can be identified with the moment of inertia defined by the angular kinetic energy in (2), $\mathcal{I} = \tfrac{4}{5}m_\alpha(r^2 + a^2) = \tfrac{4}{5}(x^2 + 1)m_\alpha a^2$, where we have approximated μ as $\tfrac{4}{5}m_\alpha$. Therefore

$$\left(\tfrac{4}{5}s^2 + 3\right) c^2 = \tfrac{4}{5}(x^2 + 1)a^2 . \quad (24)$$

When $z = 0$ and $s = \tfrac{5}{4}\sqrt{2}$, then $x = 0$, so the scale factor is $c = \sqrt{\tfrac{8}{55}} a = 2.07$ fm. The physical cluster separation is $R = sc$, and a little further algebra gives

$$R^2 = \left(x^2 + \tfrac{5}{11}\right) a^2 . \quad (25)$$

This relates the wormhole coordinate x and wormhole radius a to the physical geometry of the clusters. Note that R is not linearly related to x .

The separation of the clusters when they merge into the bipyramid is $R = \sqrt{\tfrac{5}{11}} a = 3.65$ fm. This is the same as the separation of the alpha and Oxygen-16 clusters calculated by Zhou et al. [26]. The ground state wavefunctions extend from $x = 0$ to approximately $x = 0.7$. This corresponds

to a range of R -values, between 3.65 fm and approximately 5.3 fm. The 1-phonon wavefunctions have a peak at about $x = 0.32$, corresponding to $R = 4.04$ fm, so the cluster separation hardly exceeds that of the ground state wavefunctions. In the 2-phonon wavefunctions, the node is at $x = 0.23$. The cluster separation here is $R = 3.86$ fm, so the bipyramid is only slightly split. On the other hand, the peak of the 2-phonon wavefunctions is around $x = 0.54$. Here $R = 4.68$ fm, which is a substantially larger cluster separation, larger than the sum of the root mean square radii of an alpha-particle (1.63 fm) and an Oxygen-16 nucleus (2.72 fm). This large cluster separation in the 2-phonon, higher nodal states is in agreement with what is found using a variety of microscopic cluster models, as illustrated in Fig.4.5 of ref.[14]. However, recall that our wavefunctions are only defined outside the minimal cluster separation, 3.65 fm.

5 Conclusions

We have proposed a model for the states of Neon-20 interpolating between the rotational excitations of the ground-state bipyramid, and bound states of a separated alpha-particle and a four-alpha cluster, i.e. an Oxygen-16 nucleus. The model combines a radial coordinate r , related to the cluster separation via a moment of inertia, and angular coordinates (θ, ϕ) for the spatial orientation of the axis joining the two clusters. $r = 0$ at the bipyramid.

Our significant novel idea is that the geometry of the configuration space is a 3-d spatial wormhole – an Ellis–Bronnikov wormhole – with $SO(3)$ rotational symmetry. The $SO(3)$ orbit at the wormhole throat at $r = 0$ is not a point, as in Euclidean space, but a 2-sphere of finite radius a , parametrising the orientation of the bipyramid. On the wormhole configuration space, we have added an attractive rotationally-symmetric, short-range potential, with rather simple mathematical form. The quantum states of the model are interpreted as rotational bands of the n -phonon excitations of the lowest-frequency vibrational mode of the bipyramid, which tends to produce a $1 + 4$ cluster split.

Our model differs from those based on Euclidean geometry, in that the cluster separation is never less than what it is at the bipyramid. Also, the centrifugal repulsive potential for states with non-zero angular momentum l is not singular at the bipyramid, even though $r = 0$. Another property, arising from the choice of geometry and potential, is that each rotational band has an angular momentum cut-off, and therefore only a finite number

of bound states. The threshold states at the top of the bands all have the same energy, and form a sequence of increasing angular momentum l , up to $l = 8$ for our choice of dimensionless parameter, $m = 9$. The observed Neon-20 spectrum gives support for this picture. The radial wavefunctions of the threshold states have simple analytic forms, obtained by solving an associated Legendre equation. This allows us to establish, by the Sturm oscillation theorem, exactly how many lower-lying, true bound states there are, but we have needed to find their energies numerically.

We have found that the model's energy spectrum matches the energies of observed states of Neon-20 quite well, if we calibrate the energy threshold to be at 15.19 MeV. The rotational bands include the well-established 0_1^+ ground state band, the lowest 0^- band, and the 0_4^+ band of broad, "higher nodal" states, and it supports the assignment of observed 8^+ , 7^- and 6^+ states between 15 and 16 MeV to these bands as threshold states. The calibration implies that the wormhole's throat has radius $a = 5.42$ fm, corresponding to the separation of the alpha-particle and Oxygen-16 cluster in the ground-state bipyramid being 3.65 fm.

Unlike the harmonic oscillator potential, our potential (9), shown in Fig.1, is a finite well, and it would be interesting to analyse scattering states in this potential, to determine the widths of resonant states along the lines of ref.[13], and to consider alpha/Oxygen-16 fusion [8].

A challenge is to extend the model to include further vibrational excitations of the bipyramid, and to understand theoretically all the vibrational frequencies. The geometry of such an extended model will be higher-dimensional and more complicated than a 3-d wormhole. It would also be interesting to investigate if spatial wormholes can model the excitations of other nuclei that split asymmetrically into a pair of clusters whose internal excitations can be neglected.

Acknowledgements

NSM thanks David Jenkins for helpful discussions.

References

- [1] N. S. Manton, Nonlinearity, Geometry and Field Theory Solitons, *Chapter 9* in *Emerging Frontiers in Nonlinear Science, Nonlinear Systems*

- and Complexity Vol. 32*, eds. P.G. Kevrekidis et al., Springer Nature, 2020.
- [2] J. A. Wheeler, Molecular viewpoints in nuclear structure, *Phys. Rev.* **52**, 1083 (1937).
 - [3] W. Wefelmeier, Ein geometrisches Modell des Atomkerns, *Zeit. f. Phys.* **A 107**, 332 (1937).
 - [4] L. R. Hafstad and E. Teller, The alpha-particle model of the nucleus, *Phys. Rev.* **54**, 681 (1938).
 - [5] H. G. Ellis, Ether flow through a drainhole: A particle model in general relativity, *J. Math. Phys.* **14**, 104 (1973).
 - [6] K. A. Bronnikov, Scalar-tensor theory and scalar charge, *Acta Phys. Polon.* **B 4**, 251 (1973).
 - [7] R. Bijker and F. Iachello, Cluster structure of ^{20}Ne : Evidence for \mathcal{D}_{3h} symmetry, *Nucl. Phys.* **A 1006**, 122077 (2021).
 - [8] K. Wen and T. Nakatsukasa, Adiabatic self-consistent collective path in nuclear fusion reactions, *Phys. Rev.* **C 96**, 014610 (2017).
 - [9] P. Bizoń, M. Dunajski, M. Kahl and M. Kowalczyk, Sine-Gordon on a wormhole, *Nonlinearity* **34**, 5520 (2021).
 - [10] A. Waterhouse, The ϕ^4 kink on a wormhole spacetime, [arXiv:1908.09650](https://arxiv.org/abs/1908.09650) (2019).
 - [11] Digital Library of Mathematical Functions,
<https://dlmf.nist.gov/14.7> .
 - [12] L. D. Landau and E. M. Lifshitz, *Quantum Mechanics – Course of Theoretical Physics Vol. 3 (3rd ed.)*, Butterworth–Heinemann, Oxford, 1977.
 - [13] B. Buck, C. B. Dover and J. P. Vary, Simple potential model for cluster states in light nuclei, *Phys. Rev.* **C 11**, 1803 (1975).
 - [14] Y. Fujiwara et al., Chapter 2: Comprehensive study of alpha-nuclei, *Prog. Theor. Phys. Suppl.* **68**, 29 (1980).
 - [15] TUNL Nuclear Data Project,
<https://nucldata.tunl.duke.edu> .
 - [16] D. R. Tilley et al., Energy levels of light nuclei, $A = 20$, *Nucl. Phys.* **A 636**, 249 (1988).
 - [17] Evaluated Nuclear Structure Data File,
<https://www.nndc.bnl.gov/ensdf/index.jsp> .

- [18] A. E. Litherland et al., Rotational bands in Ne^{20} , *Phys. Rev. Lett.* **7**, 98 (1961).
- [19] M. Bouten, α -particle model of ^{20}Ne and ^{24}Mg , *Nuovo Cim.* **26**, 63 (1962).
- [20] J. Cseh and G. Levai, Core-plus-alpha-particle states of ^{20}Ne and ^{16}O in terms of vibron models, *Phys. Rev. C* **38**, 972 (1988).
- [21] P. Marević et al., Quadrupole and octupole collectivity and cluster structures in neon isotopes, *Phys. Rev. C* **97**, 024334 (2018).
- [22] F. Michel, G. Reidemeister and S. Ohkubo, Last members of the $K^\pi = 0_4^+$ α -cluster rotational band in ^{20}Ne , *Phys. Rev. C* **35**, 1961 (1987).
- [23] I. Lombardo et al., New analysis of $p + ^{19}\text{F}$ reactions at low energies and the spectroscopy of natural-parity states in ^{20}Ne , *Phys. Rev. C* **100**, 044307 (2019).
- [24] C. J. Halcrow, C. King and N. S. Manton, Oxygen-16 spectrum from tetrahedral vibrations and their rotational excitations, *Int. J. Mod. Phys. E* **28**, 1950026 (2019).
- [25] N. S. Manton, Evidence for tetrahedral structure of Calcium-40, *Int. J. Mod. Phys. E* **29**, 2050018 (2020).
- [26] B. Zhou et al., Nonlocalized cluster dynamics and nuclear molecular structure, *Phys. Rev. C* **89**, 034319 (2014).